Water Resources and Industry 7-8 (2014) 23–37

Contents lists available at ScienceDirect

Water Resources and Industry

journal homepage: www.elsevier.com/locate/wri

Fe_3O_4–wheat straw: preparation, characterization and its application for methylene blue adsorption

A. Ebrahimian Pirbazari [a,b,*], E. Saberikhah [a], S.S. Habibzadeh Kozani [b]

[a] Faculty of Fouman, College of Engineering, University of Tehran, P.O. Box 43515-1155, Fouman 43516-66456, Iran
[b] Faculty of Caspian, College of Engineering, University of Tehran, P.O. Box 43841-119, Rezvanshahr 43861-56387, Iran

ARTICLE INFO

Article history:
Received 27 April 2014
Received in revised form
4 September 2014
Accepted 6 September 2014

Keywords:
Wheat straw
Nanoparticles
Methylene blue
Isotherm
Kinetic

ABSTRACT

The removal of methylene blue (MB) from aqueous solution by NaOH-treated wheat straw from agriculture biomass impregnated with Fe_3O_4 magnetic nanoparticles (MNP-NWS) was investigated. Magnetic nanoparticles (Fe_3O_4) were prepared by chemical precipitation of a mixture of Fe^{2+} and Fe^{3+} salts from solution aqueous by ammonia. These magnetic nanoparticles of the adsorbent Fe_3O_4 were characterized by Field Emission Scanning Electron Microscopy (FESEM), X-ray Diffraction (XRD), nitrogen physisorption and Fourier Transform Infrared Spectroscopy (FTIR). FTIR results showed complexation and ion exchange appears to be the principal mechanism for MB adsorption. The adsorption isotherm data were fitted to Langmuir, Sips, Redlich–Peterson and Freundlich equations. Langmuir adsorption capacity, Q_{max}, was found to be 1374.6 mgg^{-1}. The Freundlich equation yielded the best fit to the experimental data in comparison to the other isotherm models. The removal of MB by MNP-NWS followed pseudo-first-order reaction kinetics based on Lagergren equations.

1. Introduction

The treatment of industrial effluents is a challenging topic in environmental science, as control of water pollution has become of increasing importance in recent years [1–3]. Synthetic dyes are widely

* Corresponding author at: Faculty of Fouman, College of Engineering, University of Tehran, P.O. Box 43515-1155, Fouman 43516-66456, Iran. Tel.: +981327234927; fax: +981327237228.
E-mail address: aebrahimian@ut.ac.ir (A. Ebrahimian Pirbazari).

http://dx.doi.org/10.1016/j.wri.2014.09.001

used in a number of industrial processes, such as the textile industry, paper printing [3]. Although methylene blue (MB), a cationic dye, is not particularly hazardous, it can cause some harmful effects. Acute exposure to MB can cause increased heart rate, vomiting, shock, Heinz body formation, cyanosis, jaundice and quadriplegia, and tissue necrosis in humans [4,5]. Hence, the necessity for the dye-containing water to undergo treatment before disposal to the environment [6].

In spite of the availability of many techniques such as coagulation, chemical oxidation, membrane separation processes, electrochemical, aerobic and anaerobic microbial degradation for wastewaters treatment, these methods are not very successful due to suffering from many restrictions. Among all these methods, adsorption has been preferred due to its cheapness and the high quality of the treated effluents, especially for well-designed sorption processes [7]. Since the performance of an adsorptive separation is directly dependent on the quality and cost-effectiveness of the adsorbent, the last decade has seen continuous improvement in the development of effective adsorbents in the form of activated carbon [8], zeolites [9], clay minerals [10], chitosan [11], lignocelluloses [12], natural minerals [13] and functionalized polymers [14]. However, most of these adsorbents are either not effective (due to diffusion limitation or the lack of active surface sites) or have shown problems like high cost, difficulties of separation from wastewater, or generation of secondary wastes. One advanced class of adsorbent, magnetic nano-adsorbents with the help of an external magnetic field, has been further successful in circumventing the solid–liquid separation problem usually encountered with nanoparticles. Such novel adsorbent combining nanotechnology and magnetic separation technique has not only demonstrated high adsorption efficiency due to its large surface area to volume ratio, but has also shown additional benefits like ease of synthesis, easy recovery and manipulation *via* subsequent coating and functionalization, absence of secondary pollutants, cost-effectiveness and environmental friendliness [15].

Cheaper and effective adsorbents can be formed from abundant natural materials or certain waste materials (or products) from industrial and agricultural activities. In general, an adsorbent which requires little processing or is abundant in nature or is a by-product or waste material from another industry is called a “low-cost” adsorbent [3,16]. In recent years, a vast number of publications have been dedicated to the removal of methylene blue from wastewater by using adsorption techniques with different low-cost materials, such as straw-based adsorbents [17–20].

As an agricultural waste, wheat straw has a high yield every year. However, most of the wheat straw has been burnt for cooking or heating, or been left directly to decompose. Therefore, it is necessary to make the best use of wheat straw. Huang et al. have completed a comprehensive study of the components, structure and morphology of wheat straw [21,22]. Wheat straw has a vascular bundle structure, which provides additional surface area for chemical modification. It also has complicated components including lignin, hemicellulose, cellulose, pectin, protein and fatty acids. Wheat straw is abundant in hydroxyl groups. Our literature survey revealed only one report of synthesis of magnetic wheat straw for arsenic adsorption. The hydroxyl groups can provide chemical reaction sites and adsorb iron ions to grow Fe_3O_4 crystals [23].

In this study, we used the agricultural waste wheat straw as a template and treated it with NaOH (NWS), grow magnetic nanoparticles Fe_3O_4 (MNP) on its surface, and then investigated its potential application for adsorption with MB as a model toxic dye. The MNP-NWS characteristics and adsorption mechanism were examined by FESEM, XRD, FTIR, N_2 physisorption and point of zero charge (pzc).

2. Experimental

2.1. Materials

The wheat straw (WS) used in this study was obtained from a local wheat field of Ardebil in Iran. The raw material was cleaned and dried at 380 K for 24 h. The dried wheat straw was then ground and sieved into a size range of 100–500 μm. The resulting product was stored in an air-tight container before further use. The chemical composition of wheat straw was determined as follows: 43.1% cellulose, 19.31% lignin, 29.020% hemicellulose, 6.8% ash, and 1.64% ethanol/dichloromethane extractables on an oven-dry weight basis (moisture content 7.8%).

MB was purchased from Merck (No. 115943). A stock solution was prepared by dissolving 1.0 g of MB in 1 L of deionized water, and the concentrations of MB used (50–500 mg/L) were obtained by dilution of the stock. The pH of the solution was adjusted to the desired value (pH = 7) by adding a small quantity of 0.01 M HCl or 0.01 M NaOH.

2.2. Preparation of NaOH-treated wheat straw (NWS)

Raw wheat straw (RWS) was prepared as described previously. We prepared NaOH- treated wheat straw according to a method reported in the literature [24]. The dried RWS was treated in 0.05 M sodium hydroxide (NaOH) solution for 4 h. The material was then washed thoroughly with distilled water until it was neutral and dried in the oven at 333 K for 24 h. Finally, the resulting adsorbent (NWS) was stored in air-tight container for further use in the adsorption experiments.

2.3. Synthesis of magnetic wheat straw and characterization

The chemical precipitation technique has been used to prepare particles with homogeneous composition and narrow size distribution [25]. This technique is probably the most common and efficient method to obtain magnetic particles. A complete precipitation of Fe_3O_4 was achieved under alkaline conditions, while maintaining a molar ratio of Fe^{2+} to Fe^{3+}, 1:2, under an inert environment (nitrogen 99.999%). To obtain 2 g of magnetic particles, 2.1 g of $FeSO_4 \cdot 7H_2O$ and 3.1 g of $FeCl_3 \cdot 6H_2O$ were dissolved in 80 mL of double distilled water with vigorous stirring. While the solution was heated to 353 K, 10 mL of aqueous ammonia (25%) was added drop-wise. To ensure complete growth of the nanoparticle crystals, the solution was then added to 10 g of NWS and the reaction heated at 353 K for 30 min with constant stirring. The resulting suspension was cooled to room temperature and then washed three times with 50 mL double distilled water to remove unreacted chemicals. The synthesized adsorbent was tested with a magnetic rod as shown in Fig. 1, and it is clearly observed that all the iron oxide was attracted to the magnetic rod.

2.4. Characterization

The surface structure and morphology of NWS and MNP-NWS before and after MB adsorption were characterized using a Field Emission Scanning Electron Microscope (Hitachi, S4160, Cold Field Emission) at a 20 kV acceleration voltage. Prior to analysis, the samples were coated with a thin layer of gold. The XRD patterns of MNP-NWS were obtained by a diffractometer (D8-Advanced, Bruker AXS)

Fig. 1. Photograph of MNP-NWS attracted by magnet.

with Cu Kα radiation (λ=1.5406 nm) in steps of 0.03° (2θ) min^{-1} from 2θ=5° to 70°. Functional groups potentially involved in adsorption were identified by Fourier Transform Infrared Spectroscopy (Bruker Co. TENSOR 27, Germany) analysis in the region of 400–4000 cm^{-1} via the KBr pressed-disc method. Specific surface area based on nitrogen physisorption was measured by surface area measurement apparatus (SA-1100, Sibata, Japan). The samples were degassed at 353 K for 2 h prior to the sorption measurement.

2.5. Equilibrium and kinetic studies

Equilibrium studies were carried out by contacting fixed amount of MNP-NWS (0.1 g) with 100 mL of MB solution with different initial concentrations (50, 100, 200, 300, 400 and 500 mg/L) in 250 mL stoppered Erlenmeyer flasks at a temperature of 303 ± 2 K and pH 7. The procedure was repeated for temperatures 313 and 323 ± 2 K. MB concentrations were determined by spectrometry at 668 nm using a double beam UV–Vis spectrophotometer (Shimadzu, Model UV 2100, Japan). In the kinetics studies, the samples were taken at preset time intervals (every 20 min), and the concentrations of MB were measured. Desorption experiments were conducted by shaking 100 mg of adsorbent containing adsorbed MB with 100 mL of distilled-deionized water at 298 K and pH 7.0.

2.6. Isotherm modeling

The nonlinear forms of the Langmuir, Freundlich, Temkin, Sips and Redlich–Peterson isotherm models were used to analyze the equilibrium isotherm data [26]. The fitness of these models was evaluated by R^2. Matlab (version8.0.0.783) was used for the analysis.

The Langmuir adsorption isotherm assumes that adsorption takes place at specific homogeneous sites within the adsorbent and has found successful application for many processes of monolayer adsorption. The Langmuir isotherm can be written in the form (1):

$$q_e = \frac{(Q_{max} K_L C_e)}{(1 + K_L C_e)} \tag{1}$$

where q_e is the adsorbed amount of the dye, C_e is the equilibrium concentration of the dye in solution, Q_{max} is the monolayer adsorption capacity and K_L is the Langmuir adsorption constant. The Freundlich isotherm is an empirical equation as is that of Langmuir, which assumes that the adsorption occurs on heterogeneous surfaces. The Freundlich equation can be expressed as:

$$q_e = K_F C_e^{\,1/n} \tag{2}$$

where K_F (Freundlich adsorption coefficient) and 1/n are fitting constants which can be regarded approximately as the capacity and strength of adsorption, respectively.

The Sips model is an additional empirical model which has the features of both the Langmuir and Freundlich isotherms. The Sips model contains three parameters, Q_{max}, K_s and 1/n, which can be evaluated by fitting the experimental data. The Sips adsorption isotherm model can be written as follows:

$$q_e = \frac{(Q_{max} K_s C_e^{\,1/n})}{(1 + K_s C_e^{\,1/n})} \tag{3}$$

Similar to the Sips isotherm, Redlich and Peterson also proposed an isotherm with the features of the Langmuir and the Freundlich isotherms:

$$q_e = \frac{K_{rp} C_e}{(1 + \alpha_{rp} C_e^{\beta})} \tag{4}$$

In which K_{rp} and α_{rp} are the Redlich–Peterson constants, and β is basically in the range of zero to one. If β is equal to 1, the equation reduces to the Langmuir isotherm equation, while in case where the value of the term $\alpha_{rp} C_e^{\beta}$ is larger than one, the Redlich–Peterson isotherm equation can be approximated by a Freundlich-type equation.

The so-called Temkin isotherm was first developed by Temkin and Pyzhev and is based on the assumption that the heat of adsorption would decrease linearly with the increase of coverage of adsorbent:

$$q_e = \frac{RT \ln(a_t C_e)}{B} \tag{5}$$

In which R is the gas constant, the absolute temperature (T), B the constant related to the heat of adsorption and a_t is the Temkin isotherm constant. The Temkin isotherm equation has been applied to describe adsorption on heterogeneous surfaces.

2.7. Kinetic models

The Lagergren rate equation [27] is one of the most widely used adsorption rate equations for determining the adsorption of solute from a liquid solution. The pseudo-first-order kinetic model of Lagergren may be represented by:

$$\frac{dq}{q_e} - q = k_1 dt \tag{6}$$

Integrating this equation for the boundary conditions $t=0$ to $t=$t and $q=0$ to $q=q_t$ gives:

$$\ln(q_e - q_t) = \ln qe - k_1 t \tag{7}$$

where q_e and q_t are the amounts of adsorbate (mg/g) at equilibrium and at time t (min), respectively, and k_1 is the rate constant of pseudo-first-order adsorption (min^{-1}). The validity of the model can be checked by a linearized plot of $\ln(q_e - q_t)$ versus t. Also, the rate constant of pseudo-first-order adsorption is determined from the slope of the plot.

The pseudo-second-order equation based on adsorption equilibrium capacity can be expressed as:

$$\frac{dq}{(q_e - q_t)^2} = k_2 dt \tag{8}$$

Taking into account the boundary conditions $t=0$ to $t=$t and $q=0$ to $q=q_t$, the integrated linear form in the above equation can be rearranged to the following equation:

$$\frac{1}{(q_e - q_t)} - \frac{1}{q_e} = k_2 t \tag{9}$$

Rearranging the variables gives the following equation:

$$\frac{t}{q_t} = \frac{1}{k_2 q_e^2} + \frac{t}{q_e} \tag{10}$$

where the theoretical equilibrium adsorption capacity (q_e) and the second-order constants k_2 (g mg^{-1} min^{-1}) can be determined experimentally from the slope and intercept of plot t/q versus t.

2.8. Study on point of zero charge (pzc)

In the point of zero charge determination, 0.01M NaCl was prepared and its pH was adjusted in the range of 2–11 by adding 0.01M NaOH or HCl. Then, 50 mL of 0.01M NaCl each was put in conical flask and then 0.1 g of the MNP-NWS was added to these solutions. These flasks were kept for 72 h and final pH of the solution was measured by using pH meter. Graphs were then plotted for pH_{final} versus $pH_{initial}$.

3. Results and discussion

3.1. XRD, nitrogen physisorption and SEM analysis

Fig. 2 shows XRD patterns of NWS and MNP-NWS. Wheat straw consists of mainly crystalline cellulose, noncrystalline hemicellulose and lignin [28]. The diffraction peaks at $2\theta^{\circ}=16.1^{\circ}$ and 22.4° for cellulose I crystalline form, which is assigned to most natural cellulose [21]. The main crystal planes in pure Fe_3O_4 crystals ($2\theta^{\circ}=$ 19.375, 30.535, 35.695, 43.315, 57.805 and 62.935), marked by their Miller indices ((1 1 1), (2 2 0), (3 1 1), (4 0 0), (5 1 1), and (4 4 0)), were reported. The diffraction peaks of Fe_3O_4 match well with the inverse cubic spinel structure (JCPDS 19–0629). The XRD pattern of MNP-NWS confirms that the nano-Fe_3O_4 was loaded on wheat straw. The peak intensity decreases and the full width of the peak increases, which indicates the low crystallinity and small crystalline size of Fe_3O_4 particles.

The specific surface area of NWS and MNP-NWS based on nitrogen physisorption were determined by Brunauer–Emmett–Teller (BET) theory. It was found that the surface area of NWS and MNP-NWS were 22.3 and 57.5 $m^2\,g^{-1}$, respectively.

The FESEM images for the samples of the NWS, MNP-NWS before and after MB adsorption are shown in Fig. 3a to c. The NWS has insoluble cell walls with fibers largely made up of cellulose. A high response surface of the functional groups is also present. Fig. 3b shows the NWS is completely covered with iron oxide, and all the iron oxide particles are aggregated to form a spherical and cage-like structure. The presence of nano-Fe_3O_4 on the MNP-NWS surface gives a favorable paramagnetic property and is shown in Fig. 1. Fig. 3c shows the FESEM image, after MB adsorption onto MNP-NWS. Compared to Fig. 3b, more particles are present on the surface of the MNP-NWS. These are the MB dye molecules as well as the iron oxide particles.

3.2. FTIR analysis

The FT-IR spectra of MNP-NWS before and after MB adsorption are shown in Fig. 4. The peak at 668 cm^{-1} observed in Fig. 4a is related to the Fe–O group and the peak around 3447 cm^{-1} in the spectrum was assigned to the –OH group on the surface of the magnetite [22]. These two significant bands in the spectrum indicate the possible involvement of those functional groups on the surface of MNP-NWS process. Thus, it seems that this type of functional group is likely to participate in MB binding. Fig. 4b shows the FTIR spectrum after adsorption of MB onto MNP-NWS. When comparing the two spectra of Fig. 4a and b, Fig. 4b shows that the hydroxyl groups are present at 3429 cm^{-1}. This peak has shifted and changes the region of the peaks (showed with an asterisk), because the hydroxyl groups are

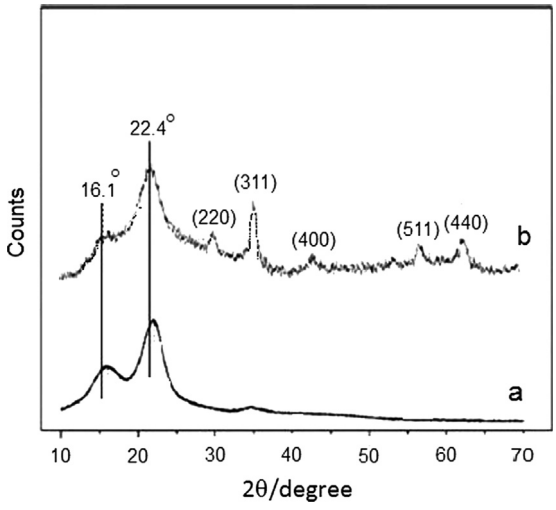

Fig. 2. XRD pattern of (a) NWS and (b) MNP-NWS.

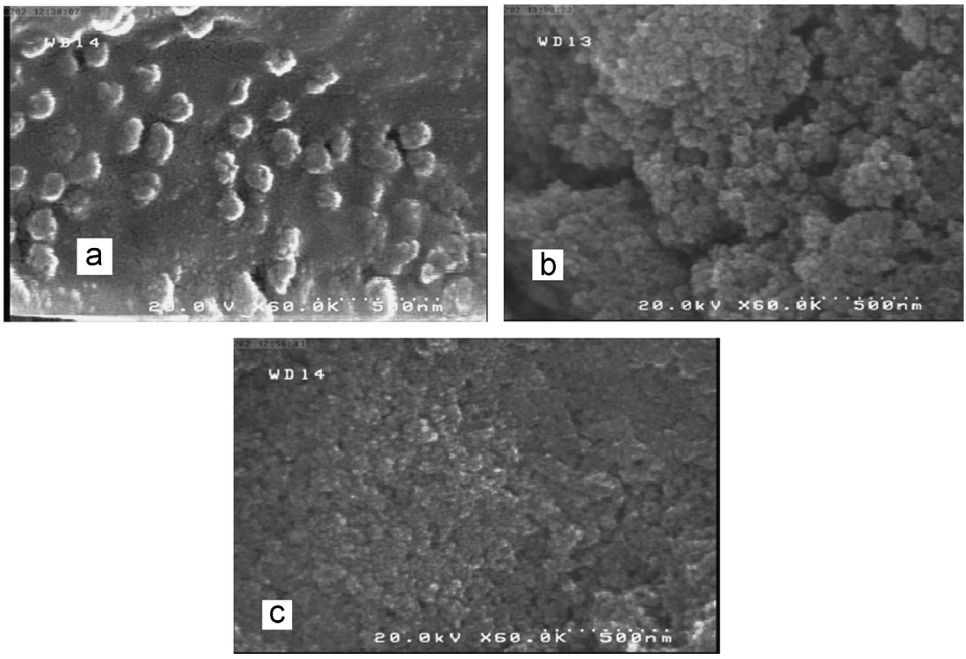

Fig. 3. FESEM images of (a) NWS, (b) MNP-NWS and (c) MNP-NWS after MB adsorption.

likely to participate in the MB adsorption. Also, peaks at 1459 and 1053 cm^{-1} (Fig. 4b) show the presence of MB dye on MNP-NWS. FTIR spectrum of MB (spectrum not shown) shows vibrations at 1444 and 1040 cm^{-1}. These peaks have shifted and change the region of the peaks because of the interaction with functional groups of MNP-NWS. A well-known mechanism involved in the adsorbate and adsorbent interaction is governed by ion exchange followed by the adsorption process. In the adsorption process, H^+ ions leaving groups of the adsorbent bind with MB^+ at the adsorbent surface due to electrostatic attraction. We will discuss the adsorption mechanism in Section 3.4.

3.3. Effect of adsorbent dose

Adsorbent dose is an important parameter that strongly influences the adsorption process by affecting the adsorption capacity of the adsorbent [29]. Therefore, the influence of adsorbent dose on MB adsorption by MNP-NWS was investigated in the range of 0.01–0.2 g/100 mL of MB solution (initial concentration: 100 mg/L) (Fig. 5). The adsorption efficiency increased from 36% to 96% as the adsorbent dose increased from 0.01 to 0.1 g. The increase in the percentage of dye removal with adsorbent dose could be attributed to an increase in the adsorbent surface area, augmenting the number of adsorption sites available for adsorption, as previously reported [30,31]. The decrease in sorption capacity with increasing dosage of adsorbent at constant dye concentration and volume may be attributed to saturation of adsorption sites due to particulate interaction such as aggregation [32]. Such aggregation would lead to a decrease in total surface area of the adsorbent and an increase in diffusional path length [33]. Therefore, in the following experiments, the adsorbent dose was fixed at 1 g/L.

3.4. Effect of pH and underlying mechanism

Fig. 6 gives the adsorption capacity of MB within pH range of 2.0–12.0. The uptake of MB increased with the increase in the solution pH and the maximum uptake of MB was observed at pH 7.0. According to the acid–base equilibrium of MB represented by $MBH^{2+} \leftrightarrows MB^+ + H^+$ and its very low p*K*a value (less than 1), the removal of MB was due mainly to solubilization of unprotonated form of the dye MB^+ [34]. At low pH

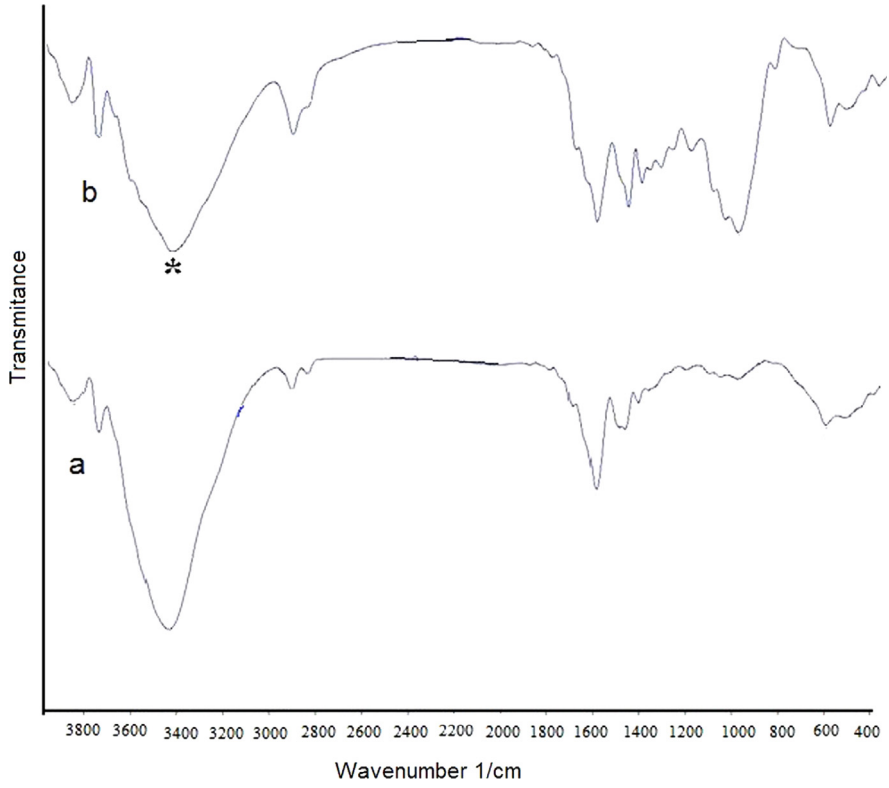

Fig. 4. FTIR spectra of MNP-NWS (a) before and (b) after MB adsorption.

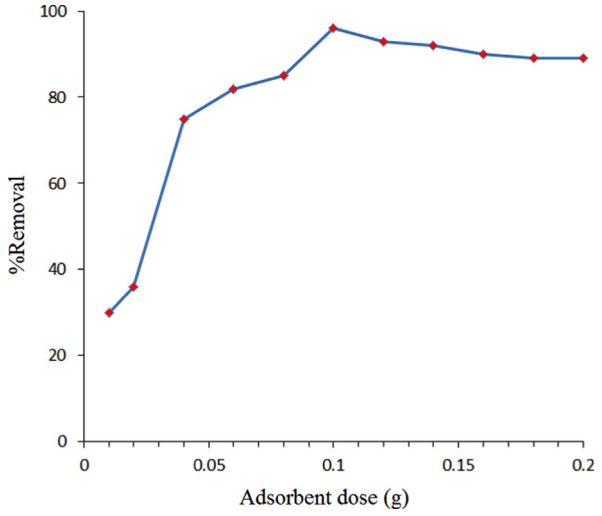

Fig. 5. Effect of adsorbent dosage on adsorption of MB (Initial MB concentration: 100 mg/L; solution volume: 100 mL, contact time: 70 min; adsorbent dose: 0.01–0.2 (g/100 mL), temperature: 298 K).

values, the poor adsorption of MB could be due to competition with the H^+ ions for binding sites on MNP-NWS. Moreover, many protons will be available to protonate the MNP-NWS surface in the condition; thereby the electrostatic repulsion between positively charged MB^+ and positively charged adsorption sites

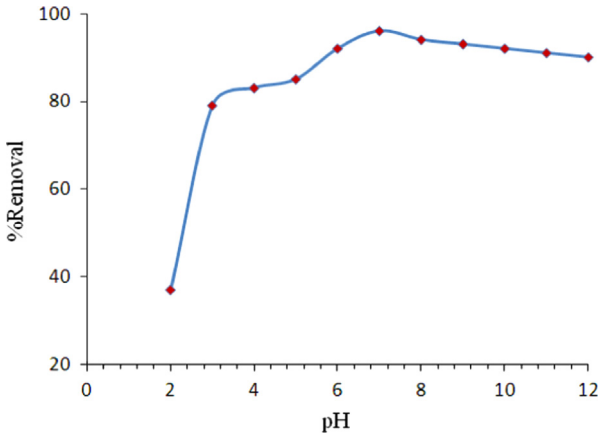

Fig. 6. Effect of pH on adsorption of MB (pH: 2–12; initial MB concentration: 100 mg/L; contact time: 70 min; adsorbent dosage: 0.1 g/100 mL; temperature: 298 K).

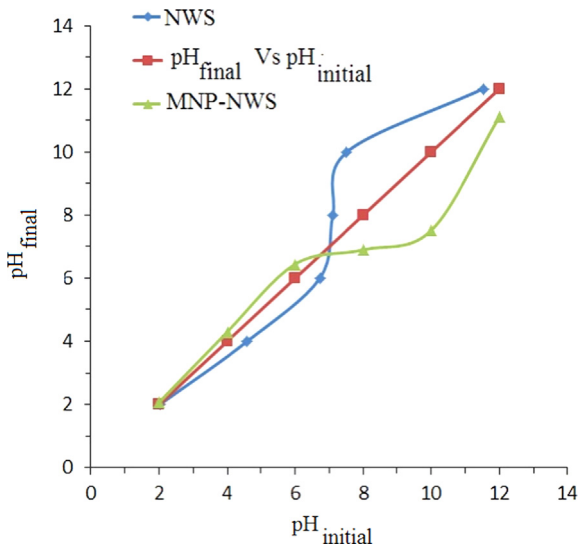

Fig. 7. Plot for determination of point zero charge of MNP-NWS.

causes the decrease in the dye adsorption. As the pH increased, the MNP-NWS surface was more negatively charged and the functional groups (such as carboxyl (pK_a= 4.02), amino (pK_a=9.39) and hydroxyl (pK_a=8.36) groups) would be less protonated [2]. Thus attraction of MB^+ was enhanced. From the point of zero charge, given in Fig. 7, the surface of MNP-NWS becomes positively charged at pH < 6.2 and at pH > 6.2, becomes progressively more negatively charged. According to the report by Wang et al. [2], at pH < pHpzc, the weak physical forces such as hydrogen bonding, van der Waals' interactions and the chemisorption might be involved in the adsorption process. They also suggested from potentiometric titration results that the carboxyl, amine and hydroxyl groups mainly present on adsorbent are responsible for dye biosorption, and the outcome verifies the results of IR analysis.

The results obtained can be explained by the effect of the surface charge of the adsorbent and pzc as reported by Gupta and Nyaka [15]. The multiple hydroxyl groups on MNP–NWS as revealed by FTIR spectra play a dominant role in the MB adsorption. Depending upon the solution pH, the adsorbent surface undergoes protonation or deprotonation [15,35].

The protonation/deprotonation reaction that MNP-NWS undergoes is as follows:

$$-Fe-O-(C=O)-(OH)_n + H^+ \leftrightarrows -Fe-O-(C=O)-(OH_2)_n^+ \quad (11)$$

At pH < pHpzc (pzc of MNP–NWS is at pH = 6.2) $-Fe-O-(C=O)-(OH_2)_n^+$ are the dominant species for MNP–NWS. These species having high positive charge density make the MB^+ adsorption unfavorable due to electrostatic repulsion. Also, strict competition between H^+ and MB^+ for the active sites will decrease MB^+ adsorption [36]. But, at pH > pHpzc, $-Fe-O-(C=O)-(OH)_n$ are the dominant species in MNP–NWS. Such deprotonated species undergo electrostatic attraction for MB^+ that result in the formation of MB-Fe_3O_4 magnetic composite complexes. At this step, H^+ ions leaving functional groups of the adsorbent bind with MB^+ at the adsorbent surface due to electrostatic attraction. This causes

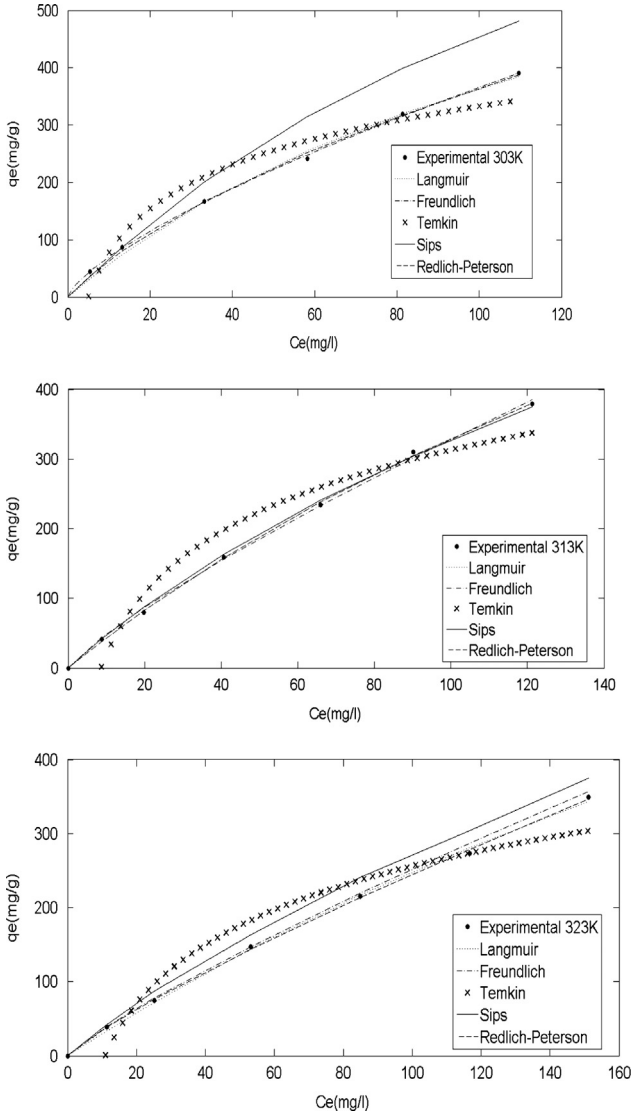

Fig. 8. Isotherm plots for MB adsorption onto MNP-NWS at different temperatures.

enhanced adsorption. Complexation and ion exchange appear to be the principle mechanism of the adsorption as revealed by Eq. (12).

$$-Fe-O-(C=O)-(OH)_n + MB^+ \rightarrow -Fe-O-(C=O)-(O\text{-}MB)_n^+ + nH^+ \quad (12)$$

3.5. Isotherm modeling

Fig. 8 and Table 1 show the fitting parameters for the measured isotherm data for MB adsorption onto MNP-NWS in the nonlinear forms of the Langmuir, Freundlich, Temkin, Redlich–Peterson and Sips models. The values of R^2 for the Langmuir, Sips, Freundlich and Redlich–Peterson models indicate good fit to four of the models. The applicability of Langmuir, Sips and Redlich-–Peterson isotherms showed that there were effectively monolayer sorption and a homogeneous distribution of active sites on the surface of the adsorbent. At all the temperatures, the Temkin isotherm represented the poorest fit of to experimental data in comparison to the other isotherm models.

The Freundlich equation yielded the best fit to the experimental data in comparison to the other equations in this study. The Freundlich equation is suitable for homogeneous and heterogeneous surfaces, indicating a multilayer adsorption [37]. The magnitude of the Freundlich constant n gives a measure of favorability of adsorption. Values of $n > 1$ represent a favorable adsorption process [29]. For the present study, the value of n also presents the same trend at all the temperatures indicating the favorable nature of adsorption of MB by MNP-NWS.

The value of exponent 1/n for the Sips model is close to unity indicating that adsorptions are homogeneous [26[. Also, there is similarity between Q_{max} values obtained from the Langmuir and Sips models at all temperatures. The monolayer capacity (Q_{max}) is 1374.6 mgg^{-1} as calculated from Langmuir or Sips models at 50 °C. The adsorption capacities of magnetic nanoparticle impregnated to wheat straw (MNP-NWS) used in the present studies are significant.

These suggest that the adsorption of MB on the MNP-NWS mainly takes place at specific for homogeneous and heterogeneous surfaces, indicating a multilayer adsorption, which well explains that the increase in MB adsorption on MNP-NWS is due to increased surface area of MNP-NWS

Table 1
Isotherm parameters for MB adsorption onto MNP-NWS.

Temperature (K)	303	313	323
Langmuir			
$Q_{max}(mgg^{-1})$	897.4	1308.4	1374.6
K_L(L/mg)	0.0068	0.0034	0.0022
R^2	0.9939	0.9993	0.9981
Freundlich			
n	1.39	1.21	1.18
K_F $(mg/g)(dm^3/mg)^{1/n}$	13.32	7.37	5.08
R^2	0.9993	0.9981	0.9993
Temkin			
B/RT	0.009	0.008	0.009
k_T(L/mg)	0.199	0.116	0.092
R^2	0.9223	0.9283	0.9283
Sips			
Q_{max} (mgg^{-1})	897.7	1308.4	1374.3
K_s $((mg^{-1})^{-1/n})$	0.0057	0.0042	0.0026
1/n	1.04	0.95	0.96
R^2	0.9919	0.9980	0.9980
Redlich-Peterson			
K_{rp} $(L.\ kg^{-1})$	8.496	4.431	14.210
α_{rp} $(kg.\ mg^{-1})$	0.0854	0.0036	1.9620
β	0.5964	0.9857	0.1942
R^2	0.9976	0.9993	0.9993

compared to NWS. The manufacture of this adsorbent could be upscaled and produced in small-scale industries.

3.6. Adsorption kinetics studies

The transient behavior of the dye adsorption process was analyzed by using the pseudo-first and pseudo-second-order kinetic models. Plotting $\ln(q_e - q_t)$ against t permits calculation of k_1 (Fig. 9a). The rate constants, k_1, evaluated from these plots with the correlation coefficients obtained are listed in Table 2. Plotting t/q against t (Fig. 9b) gives a straight line where k_2 can be calculated. The R^2 values for the pseudo-first-order kinetic model were between 0.991 and 0.993. The R^2 values for pseudo-second-order model were < 0.991, which is lower than the R^2 values obtained for the pseudo-first-order model. Therefore, the adsorption kinetics could well be satisfactorily more favorably described by pseudo-first-order kinetic model for MB adsorption onto MNP-NWS.

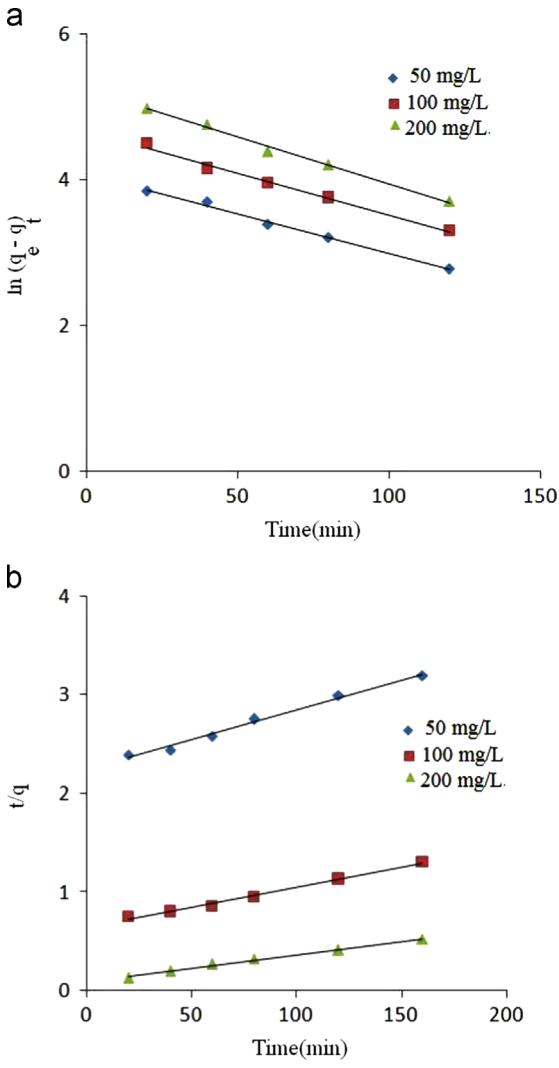

Fig. 9. Kinetic models for adsorption of MB onto MNP-NWS. (a) pseudo-first-order and (b) pseudo-second-order rate equations.

Table 2
Kinetic parameters for the adsorption of MB onto MNP-NWS based on Lagergren rate equation.

C_0 (mg/L)	Pseudo-first order			Pseudo-second order		
	q_e(mg/g)	k_1 (1/min)	R^2	q_e(mg/g)	k_2(g/mg.min)	R^2
50	58.85	0.010	0.993	166	1.6×10^{-6}	0.895
100	106.05	0.011	0.992	250	2.5×10^{-5}	0.989
200	184.74	0.012	0.991	500	4.5×10^{-5}	0991

Table 3
Comparison of the Q_{max} based on Langmuir isotherm of MB on various adsorbents.

Adsorbent	**Q_{max}(mg/g)**	**Reference**
MNP-NWS	1374.6	This work
Wheat straw	57.2	[19]
Carboxymethylation wheat straw	266.7	[19]
NaOH- modified rejected tea	242.11	[24]
Fe_3O_4-maize cob	70.29	[38]
Citric acid treated wheat straw	450	[39]
Modified rice straw	208.33	[40]

3.7. MB desorption studies

The tests of MB desorption were conducted with three initial MB concentrations (50, 100 and 200 mg/L). The MB desorbability can be defined as the ratio of the desorbed MB over the total adsorbed MB by the adsorbent. Therefore, the desorbability of MB can be used to indicate the degree of MB desorption from the adsorptive materials. The obtained data show that the desorbability of MB is about 9–12%, and the amount of the desorbed MB is slightly increased with the increase of the adsorbed MB. These results indicate that the MB adsorption on the MNP-NWS is not completely reversible and the bonding between the MNP-NWS and adsorbed MB is likely strong. It is relatively difficult for the adsorbed MB to be desorbed from the MNP-NWS.

3.8. Comparison with other bioadsorbents

A comparison of the maximum adsorption capacity (Q_{max} value) of MNP-NWS with those of other low-cost adsorbents in the literatures is shown in Table 3. The MNP-NWS shows the comparable adsorption capacity for MB with respect to other low-cost adsorbents. However, the adsorption capacity was higher than those of other adsorbents. Therefore, MNP-NWS is suitable and promising for MB removal from aqueous solutions since it has a relatively high adsorption capacity and was easily recovered from treated effluents by applying a magnet.

4. Conclusion

The efficiency of magnetic nanoparticle Fe_3O_4 (MNP) impregnated onto NaOH-treated wheat straw in removing methylene blue dye from aqueous solution has been investigated. Results indicate that adsorption is pH and temperature dependent. The adsorption isotherm data were fitted to the Langmuir, Sips, Redlich–Peterson and Freundlich isotherms. The adsorption capacity based on Langmuir isotherm was found to be 1374.6 mgg^{-1}. Adsorption followed pseudo-first-order kinetics. The removal efficiency increases with temperature and hence the adsorption process is endothermic in nature. The developed MNP–NWS has not only demonstrated higher adsorption efficiency and fast kinetics but also shows additional benefits like ease of synthesis, easy recovery, absence of secondary pollutants, cost-effectiveness

and environmental-friendliness. It can be concluded to be a promising advanced adsorbent in environmental pollution cleanup

Acknowledgment

The authors wish to acknowledge the financial support of the University of Tehran.

References

[1] V. Rocher, J.L. Siaugue, V. Cabuil, A. Bee, Removal of organic dyes by magnetic alginate beads, Water Res. 42 (2008) 1290–1298.
[2] Y. Tian, C. Ji, M. Zhao, M. Xu, Y. Zhang, R. Wang, Preparation and characterization of baker's yeast modified by nano-Fe_3O_4: application of biosorption of methyl violet in aqueous solution, Chem. Eng. J. 165 (2010) 474–481.
[3] M. Rafatullah, O. Sulaiman, R. Hashim, A. Ahmad, Adsorption of methylene blue on low-cost adsorbents: a review, J. Hazard. Mater. 177 (2010) 70–80.
[4] K.V. Kumar, V. Ramamurthi, S. Sivanesan, Modeling the mechanism involved during the sorption of methylene blue onto fly ash, J. Colloid Interf. Sci. 284 (2005) 14–21.
[5] M.T. Uddin, M.A. Islam, S. Mahmud, M. Rukanuzzaman, Adsorptive removal of methylene blue by tea waste, J. Hazard. Mater. 164 (2009) 53–60.
[6] N. Nasuha, B.H. Hameed, A.T. Mohd Din, Rejected tea as a potential low-cost adsorbent for the removal of methylene blue, J. Hazard. Mater. 175 (2010) 126–132.
[7] M.A. Salleh, D.K. Mahmoud, W.A. Karim, A. Idris, Cationic and anionic dye adsorption by agricultural solid wastes: a comprehensive review, Desalination 280 (2011) (2011) 1–13.
[8] M.S. Shafeeyan, W.M. Ashri Wan Daud, A. Houshm, A. Shamiri, A review on surface modification of activated carbon for carbon dioxide adsorption, J. Anal. Appl. Pyrol. 89 (2010) 143–151.
[9] M.R. Panuccio, A. Sorgonà, M. Rizzo, G. Cacco, Cadmium adsorption on vermiculite, zeolite and pumice: batch experimental studies, J. Environ. Manage. 90 (2009) 364–374.
[10] J. Hizal, R. Apak, Modeling of cadmium (II) adsorption on kaolinite-based clays in the absence and presence of humic acid, Appl. Clay Sci. 32 (2006) 232–244.
[11] J.T. Bamgbose, S. Adewuyi, O. Bamgbose, A.A. Adetoye, Adsorption kinetics of cadmium and lead by chitosan, Afr. J. Biotechnol. 9 (2010) 2560–2565.
[12] E.W. Shin, K.G. Karthikeyan, M.A. Tshabalala, Adsorption mechanism of cadmium on juniper bark and wood, Bioresource Technol. 98 (2007) 588–594.
[13] K. Sevgi, Adsorption of Cd(II), Cr(III) and Mn(II) on natural sepiolite, Desalination 244 (2009) 24–30.
[14] G.C. Panda, S.K. Das, A.K. Guha, Biosorption of cadmium and nickel by functionalized husk of Lathyrussativus, Colloid Surface B 62 (2008) 173–179.
[15] V.K. Gupta, A. Nayak, Cadmium removal and recovery from aqueous solutions by novel adsorbents prepared from orange peel and Fe_2O_3 nanoparticles, Chem. Eng. J. 180 (2012) 81–90.
[16] V.K. Gupta, Suhas, application of low-cost adsorbents for dye removal – a review, J. Environ. Manage. 90 (2009) 2313–2342.
[17] W. Zhang, H. Yang, L. Dong, H. Yan, H. Li, Z. Jiang, X. Kan, A. Li, R. Cheng, Efficient removal of both cationic and anionic dyes from aqueous solutions using a novel amphoteric straw-based adsorbent, Carbohyd. Polym. 90 (2012) 887–893.
[18] W. Zhang, H. Li, X. Kan, L. Dong, H. Yan, Z. Jiang, H. Yang, A. Li, R. Cheng, Adsorption of anionic dyes from aqueous solutions using chemically modified straw, Bioresource Technol. 117 (2012) 40–47.
[19] W. Zhang, H. Yan, H. Li, Z. Jiang, L. Dong, X. Kan, H. Yang, A. Li, R. Cheng, Removal of dyes from aqueous solutions by straw based adsorbents: batch and column studies, Chem. Eng. J. 168 (2011) 1120–1127.
[20] W. Zhang, L. Dong, H. Yan, H. Li, Z. Jiang, X. Kan, H. Yang, A. Li, R. Cheng, Removal of methylene blue from aqueous solutions by straw based adsorbents in a fixed-bed column, Chem. Eng. J. 173 (2011) 429–436.
[21] R. Liu, H. Yu, Y. Huang, Structure and morphology of cellulose in wheat straw, Cellulose 12 (2005) 25–34.
[22] H. Yu, R. Liu, D. Shen, Y. Jiang, Y. Huang, Study on morphology and orientation of cellulose in the vascular bundle of wheat straw, Polymer 46 (2005) 5689–5694.
[23] Y. Tian, M. Wu, Xi. Lin, P. Huang, Y. Huang, Synthesis of magnetic wheat straw for arsenic adsorption, J. Hazard. Mater. 193 (2011) 10–16.
[24] N. Nasuha, B.H. Hameed, Adsorption of methylene blue from aqueous solution onto NaOH-modified rejected tea, Chem. Eng. J. 166 (2011) 783–786.
[25] S. Laurent, D. Forge, M. Port, A. Roch, C. Robic, L. Vander Elst, R.N. Muller, Magnetic iron oxide nanoparticles: synthesis, stabilization, vectorization, physicochemical characterizations and biological applications, Chem. Rev. 108 (2008) 2064–2110.
[26] Y. Liu, Y.J. Liu, Biosorption isotherms, kinetics and thermodynamics, Sep. Purif. Technol. 61 (2008) 229–242.
[27] S. Lagergren, B.K Svenska, Zur theorie der sogenannten adsorption geloster stoffe, Vetenskapsakad, Handling 24 (1898) 1–39.
[28] P. Panneerselvam, N. Morad, K.A. Tan, Magnetic nanoparticle (Fe_3O_4) impregnated onto tea waste for the removal of nickel (II) from aqueous solution, J. Hazard. Mater. 186 (2011) 160–168.
[29] S. Chakraborty, S. Chowdhury, P.D. Saha, Adsorption of crystal violet from aqueous solution onto NaOH-modified rice husk, Carbohyd. Polym. 86 (2011) 1533–1541.
[30] A. Ahmad, Studies on adsorption of crystal violet dye from aqueous solution onto coniferous pinus bark powder (CPBP), J. Hazard. Mater. 171 (2009) 767–773.

[31] A. Saeed, M. Sharif, M. Iqbal, Application potential of grapefruit peel as dye sorbent: kinetics, equilibrium and mechanism of crystal violet adsorption, J. Hazard. Mater. 179 (2010) 564–572.
[32] O. Aksakal, H. Ucun, Equilibrium, kinetic and thermodynamic studies of the biosorption of textile dye (Reactive Red 195) onto Pinus sylvestris L, J. Hazard. Mater. 181 (2010) 666–672.
[33] G. Crini, H.N. Peindy, F. Gimbert, C. Robert, Removal of C.I. Basic Green 4 (Malachite Green) from aqueous solutions by adsorption using cyclodextrin-based adsorbent: kinetic and equilibrium studies, Sep. Purif. Technol. 53 (2007) 97–110.
[34] N. Zaghbani, A. Hafiane, M. Dhahbi, Separation of methylene blue from aqueous solution by micellar enhanced ultrafiltration, Sep. Purif. Technol. 55 (2007) 117–124.
[35] S.S. Banerjee, D.H. Chen, Fast removal of copper ions by gum arabic modified magnetic nano-adsorbent, J. Hazard. Mater. 147 (2007) 792–799.
[36] H. Yong-Meia, C. Mana, H. Zhong-Bob, Effective removal of Cu (II) ions from aqueous solution by amino-functionalized magnetic nanoparticles, J. Hazard. Mater. 184 (2010) 392–399.
[37] J.C. Igwe, A.A. Abia, Maize cob and husk as adsorbent for removal Cd, Pb and Zn ions from wastewater, Phys. Sci. 2 (2003) 83–94.
[38] K.A. Tan, N. Morad, T.T Teng, I. Norli, P. Panneerselvam, Removal of cationic dye by magnetic nanoparticle (Fe_3O_4) impregnated onto activated maize cob powder and kinetic study of dye waste adsorption, APCBEE Procedia 1 (2012) 83–89.
[39] R. Han, L. Zhang, C. Song, M. Zhang, H. Zhu, L. Zhang, Characterization of modified wheat straw, kinetic and equilibrium study about copper ion and methylene blue adsorption in batch mode, Carbohyd. Polym. 79 (2010) 1140–1149.
[40] R Gong, Y. Jin, J. Chen, Y. Hu, J. Sun, Removal of basic dyes from aqueous solution by sorption on phosphoric acid modified rice straw, Dyes Pigments 73 (2007) 332–337.